IEICE TRANS. ELECTRON., VOL.E94–C, NO.8 AUGUST 2011

BRIEF PAPER

Multi-Static UWB Radar Approach Based on Aperture Synthesis of Double Scattered Waves for Shadow Region Imaging

Shouhei KIDERA[†a)] ***and*** **Tetsuo KIRIMOTO**[†]**,** ***Members***

SUMMARY The applicability in harsh optical environments, such as dark smog, or strong backlight of ultra-wide band (UWB) pulse radar has a definite advantage over optical ranging techniques. We have already proposed the extended Synthetic Aperture Radar (SAR) algorithm employing double scattered waves, which aimed at enhancing the reconstructible region of the target boundary including shadow region. However, it still suffers from the shadow area for the target that has a sharp inclination or deep concave boundary, because it assumes a mono-static model, whose real aperture size is, in general, small. To resolve this issue, this study proposes an extension algorithm of the double scattered SAR based on a multi-static configuration. While this extension is quite simple, the effectiveness of the proposed method is nontrivial with regard to the expansion of the imaging range. The results from numerical simulations verify that our method significantly enhances the visible range of the target surfaces without *a priori* knowledge of the target shapes or any preliminary observation of its surroundings.

key words: *UWB radars, multiple scattered waves, SAR, shadow region imaging, multi-static radar, complex-shaped or multiple targets*

1. Introduction

UWB radar with high range resolution enables various applications for near field sensing. It is applicable to non-contact measurement such as manufacturing reflector antennas or aircraft bodies that have high-precision and specular surfaces, or spatial measurement for rescue or resource exploration robots that can identify a human body or materials even in darkness, smog or high-concentration gas. Moreover, it is promising for intruder detection or elderly care in a private room, whereas an optical camera generates the unavoidable problem of an invasion of privacy.

Various kinds of radar algorithms have been developed that are aimed at geosurface measurement, landmine detection, non-destructive testing or indoor sensing, based on aperture synthesis [1] or the time reversal approach [2]. Different approaches aimed at clear boundary extraction by using the reversible transform BST (Boundary Scattering Transform) between the range wavefront and the target boundary [3], or directly reconstructing a complex-shaped target boundary using range points migration [4], are also promising for real-time and super-resolution radar imaging. However, they all have the inherent problem that the baseline length theoretically limits the reconstructible range of radar imagery. In many cases, the greater part of the target shape, such as the side of target, falls into a shadow region, which is never reconstructed since only the single scattered components are used for imaging.

To overcome this problem, we have already proposed the imaging algorithm called double scattered SAR [5]. This is based on the principle that the double scattered signal includes additional independent information on the target points compared with information from a single scattered signal. In making use of the double scattered signals, this method significantly enhances the imagery range, including the region regarded as a shadow in the original SAR. Furthermore, this method does not require a priori information of surroundings or target modeling, which is necessary for other techniques using multiple scattered waves [6], [7].

It has been demonstrated that while the former approach enhances the imagery range for several target cases, the greater part of the target boundary still falls into a shadow, even when using the double scattering components. This is because it assumes a mono-static configuration, in which the real aperture size is often insufficient to recognize a target shape, especially if it has a deep-set concave shape or a sharply-inclined boundary. To overcome this difficulty, this study introduces a multi-static model using an array antenna, where the real aperture size is significantly enhanced. While this extension is quite simple, the proposed model greatly enhances the imagery range, despite the fact that the equivalent aperture size is the same as that in the mono-static model. The numerical simulation proves that the imagery range using the multi-static model expresses the target shape, which was never recognized by the former model.

2. System Model

Figure 1 illustrates the system model, where it assumes the 2-dimensional problem and TE mode waves, for simplicity. It presumes that the target has an arbitrary shape with high conductivity such as metallic objects, and a transmissive wave is ignored in this case. Moreover, the target has a clear boundary as to the conductivity, whose spatial gradient is expressed as the Dirac's delta function [3]. It also presumes that the target has an arbitrary shape with a clear boundary. The propagation speed of the radio wave, c, is assumed to be a known constant. An omni-directional antenna is used, and the transmitted current is provided by a monocycle pulse. The real space in which the target and antenna are located is expressed by the parameters $\boldsymbol{r} = (x, z)$, which

Manuscript received December 9, 2010.
Manuscript revised April 19, 2011.

[†]The authors are with the Graduate School of Informatics and Engineering, University of Electro-Communications, Chofu-shi, 182-8585 Japan.
a) E-mail: kidera@ee.uec.ac.jp

DOI: 10.1587/transele.E94.C.1320

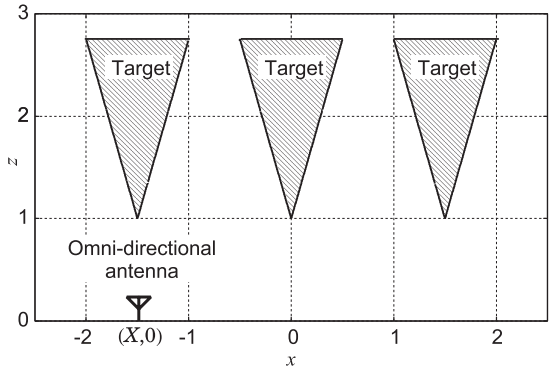

Fig. 1 System model.

are normalized by λ, the central wavelength of the pulse.

3. Conventional Model for Double Scattered SAR

The extended SAR algorithm using the double scattered signals has already been developed to enhance the imagery range, which becomes a shadow in the original SAR image [5]. This method assumes that mono-static radar is scanned along the x axis, and $s(X, Z)$ is defined as the output of the Wiener filter at the antenna location $(X, 0)$, where $Z = ct/(2\lambda)$ is expressed by the time t. The procedure for creating $s(X, Z)$ is detailed in [4]. This method is based on the simple principle that, "a double scattered wave propagates a different path from that of a single scattered one, and this wave often includes significant information on two reflection points on the target boundaries". The suitable use of multiple scattered signals is promising for shadow region imaging. It calculates the image migrated by double scattered signals as

$$I_2^{\mathrm{S}}(\boldsymbol{r}) = -\int_{\boldsymbol{r}'\in R}\int_{X\in\Gamma} I_1^{\mathrm{S}}(\boldsymbol{r}')\quad s\left(X, d(\boldsymbol{r},\boldsymbol{r}',X,X)/2\right) \times \mathrm{d}X\mathrm{d}x'\mathrm{d}z', \tag{1}$$

where Γ is the scanning range of the antenna, $\boldsymbol{r}' = (x', z')$ is defined, R is the region of the real space, and $d(\boldsymbol{r}, \boldsymbol{r}', X, X') = \sqrt{(x-X)^2+z^2} + \sqrt{(x'-X')^2+z'^2} + \sqrt{(x-x')^2+(z-z')^2}$ holds. The minus sign of the right term in Eq. (1) creates a positive image focused by double scattered waves, which have an anti-phase relationship compared with single scattered waves. The initial image $I_1^{\mathrm{S}}(\boldsymbol{r})$ is defined as the original SAR image by

$$I_1^{\mathrm{S}}(\boldsymbol{r}) = \int_{X\in\Gamma} s\left(X, d(\boldsymbol{r},\boldsymbol{r},X,X)/2\right)\mathrm{d}X, \tag{2}$$

Equation (1) expresses the aperture synthesis of the received signals by considering only a double scattered path. The final image is defined as

$$I^{\mathrm{S}}(\boldsymbol{r}) = \frac{I_1^{\mathrm{S}}(\boldsymbol{r})H(I_1^{\mathrm{S}}(\boldsymbol{r}))}{\max_{\boldsymbol{r}} I_1^{\mathrm{S}}(\boldsymbol{r})} + \frac{I_2^{\mathrm{S}}(\boldsymbol{r})H(I_2^{\mathrm{S}}(\boldsymbol{r}))}{\max_{\boldsymbol{r}} I_2^{\mathrm{S}}(\boldsymbol{r})}, \tag{3}$$

where $H(*)$ is the Heaviside function. This method directly

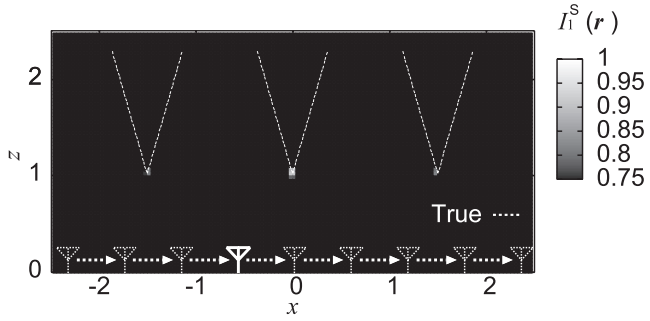

Fig. 2 Estimated image $I_1^{\mathrm{S}}(\boldsymbol{r})$, where mono-static model is assumed.

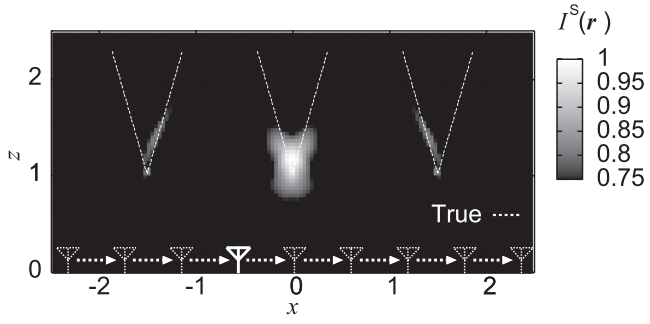

Fig. 3 Estimated image $I^{\mathrm{S}}(\boldsymbol{r})$, where multi-static model is assumed.

enhances the imagery range with only a single observation, and does not require any priori information on surroundings, or target modeling, which are substantial advantages for the other algorithms [6], [7].

An example of this method is presented as follows. The received signals are calculated by the FDTD method, and obtained at 401 locations in the range, $-2.5 \le X \le 2.5$. The target boundary is assumed as shown in Fig. 1. Figures 2 and 3 show $I_1^{\mathrm{S}}(\boldsymbol{r})$ and $I^{\mathrm{S}}(\boldsymbol{r})$. Each image is normalized by its maximum value. $I_1^{\mathrm{S}}(\boldsymbol{r})$ expresses only the convex edges of the triangle boundary because only single scattered signals are used for imaging. In addition, Fig. 3 shows that the triangle side of the target is still not reconstructed, despite the use of double scattered waves. This is because the double scattered signals, which propagate on the sharp inclined side of the triangles, are not observed for any antenna location. The above result suggests that, to enhance the imagery range, a sufficiently large real aperture size is required.

4. Proposed Model for Double Scattered SAR

To outperform the former algorithm, we propose using the multi-static configuration for the multiple scattered SAR, which can enhance a real aperture size. Figures 4 and 5 show the scattering center points when using mono-static and multi-static models, respectively. The number of array antennas is 26, for $-2.5 \le x \le 2.5$, whose combination number as ${}_{26}\mathrm{C}_2 = 325$ is less than the number of scanning samples in mono-static model of 401. Each scattering center point is calculated using the geometrical optics, considering that the propagation path is secluded from other targets [5].

In the mono-static model as shown in Fig. 4, there are a few points around the lower side of the triangle boundaries, but most of the scattering center points are concentrated on the edges. It is confirmed that the locations of these points are focused in the same region, even if the number of scanning samples increases. Conversely, in the multi-static model, the number of scattering center points around the side of each triangle increases noticeably, and the central target shape can be identified as part of the triangle, despite an aperture size which is equivalent to that in the previous model. This is because the combination of the transmitting and receiving antennas creates different scattering paths, and increases the number of independent target points. This reveals that the extension for the multi-static model offers a substantial improvement, which is a unique characteristic for double scattering propagation.

Here, the transmitting and receiving antenna locations are defined as $(X_\mathrm{T}, 0)$ and $(X_\mathrm{R}, 0)$, respectively. In each combination of X_T and X_R, the output of the Wiener filter is redefined as $s(X_\mathrm{T}, X_\mathrm{R}, Z)$. The previous work is readily extended to the multi-static model, and the estimated image with this model as $I_2^\mathrm{A}(\boldsymbol{r})$ is calculated as,

$$I_2^\mathrm{A}(\boldsymbol{r}) = -\int_{\boldsymbol{r}'\in R}\int_{X_\mathrm{R}\in\Gamma}\int_{X_\mathrm{T}\in\Gamma} I_1^\mathrm{A}(\boldsymbol{r}') \times s\left(X_\mathrm{T}, X_\mathrm{R}, d(\boldsymbol{r}, \boldsymbol{r}', X_\mathrm{T}, X_\mathrm{R})/2\right) \mathrm{d}X_\mathrm{T}\mathrm{d}X_\mathrm{R}\mathrm{d}x'\mathrm{d}z', \quad (4)$$

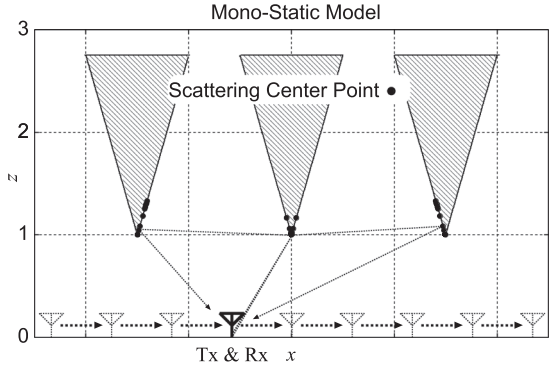

Fig. 4 Scattering center points with double scattered waves in mono-static model, where the number of scanning sample is 401.

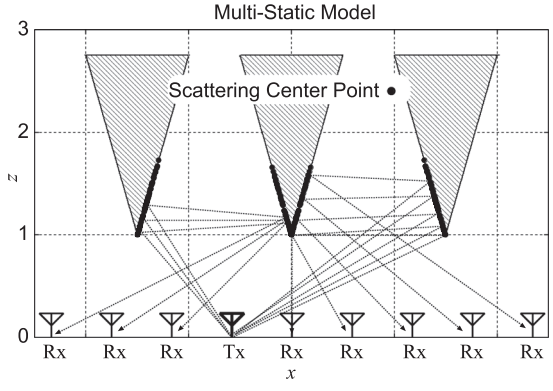

Fig. 5 Scattering center points with double scattered waves in multi-static model, where the number of array antenna is 26.

where $I_1^\mathrm{A}(\boldsymbol{r})$ is defined as,

$$I_1^\mathrm{A}(\boldsymbol{r}) = \int_{X_\mathrm{T}\in\Gamma}\int_{X_\mathrm{R}\in\Gamma} s\left(X_\mathrm{T}, X_\mathrm{R}, d(\boldsymbol{r}, \boldsymbol{r}, X_\mathrm{T}, X_\mathrm{R})/2\right) \mathrm{d}X_\mathrm{R}\mathrm{d}X_\mathrm{T}. \quad (5)$$

The final image is similarly defined by Eq. (3). This observation model significantly enhances the real aperture size. That is, it expands the visible range in spite of the fact that the baseline lengths of both the conventional and proposed models are the same.

5. Performance Evaluation

This section presents the example used in the proposed model. Figures 6 and 7 show $I_1^\mathrm{A}(\boldsymbol{r})$ and $I^\mathrm{A}(\boldsymbol{r})$ for the triangular objects, respectively. The conductivity σ_t and relative permittivity ϵ_t of the target are set to $\sigma_\mathrm{t} = 1.0 \times 10^6$ S/m and $\epsilon_\mathrm{t} = 1.0$, respectively. The number of array antennas is 26, assuming the same baseline as in Fig. 2. Figure 6 indicates that the image obtained by single scattered SAR $I_1^\mathrm{A}(\boldsymbol{r})$ does not enhance the imagery range, entirely, even if the real aperture size is enhanced. This is because it uses only the single scattered wave for imaging. Conversely, Fig. 7 reveals that the triangular side of the target is reconstructed, and offers a substantial image for identifying the triangular shapes. This is because the multi-static configuration increases the number of double scattered signals, which includes independent information on the target boundary, thus the enhanced real aperture size improves the imagery range.

Additional examples for a concave boundary target are investigated as follows. The conductivity and relative permittivity of the target are the same as in the previous case.

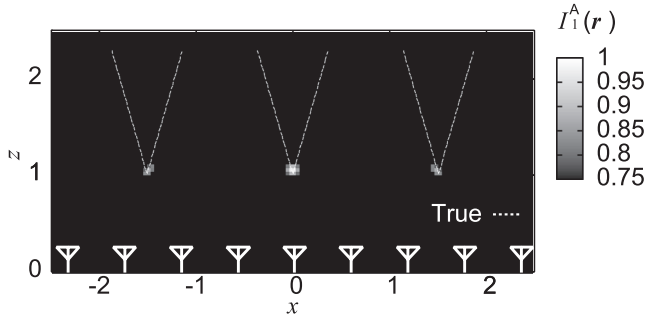

Fig. 6 Estimated image $I_1^\mathrm{A}(\boldsymbol{r})$, where multi-static model is assumed.

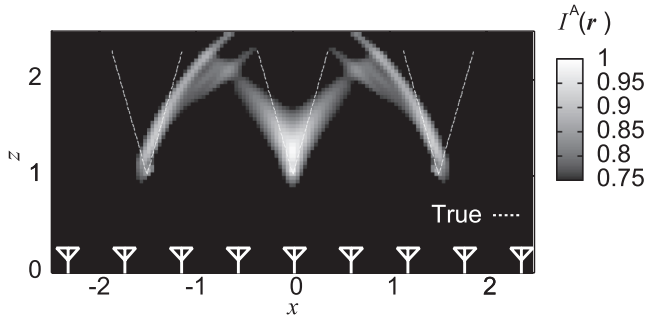

Fig. 7 Estimated image $I^\mathrm{A}(\boldsymbol{r})$, where multi-static model is assumed.

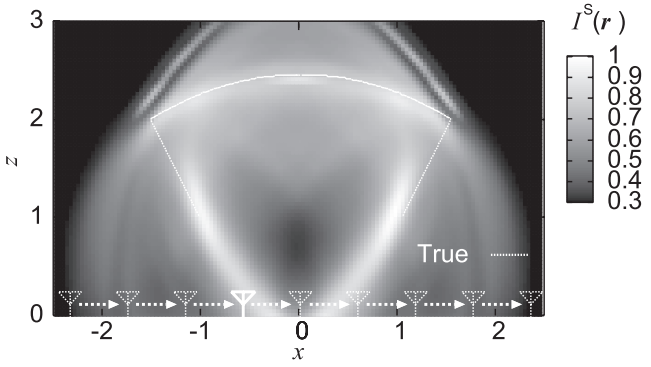

Fig. 8 Estimated image $I^S(\boldsymbol{r})$ for the concave target, where mono-static model is assumed.

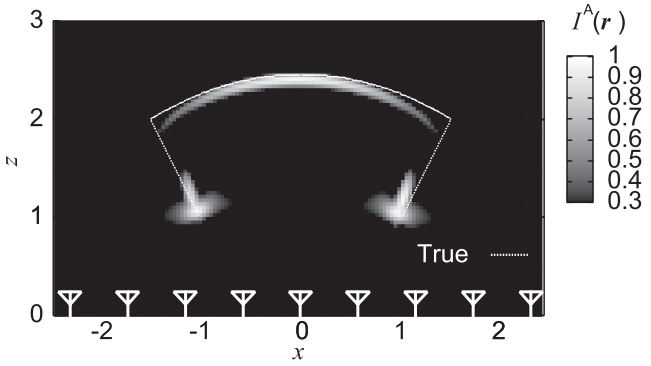

Fig. 9 Estimated image $I^A(\boldsymbol{r})$ for the concave target, where multi-static model is assumed.

Figures 8 and 9 show $I^S(\boldsymbol{r})$ and $I^A(\boldsymbol{r})$ for the concave objects, respectively. As shown in Fig. 8, there are many false images far from the actual target boundary because the received signals from the side of the target cannot be observed in any antenna location in this model. Then, the conventional model cannot offer a significant focal image, and unnecessarily illuminates the nonboundary region by the normalization in Eq. (3). In contrast, the image obtained by the proposed model in Fig. 9 enhances the visible range of the side of the target, while the false images are effectively suppressed.

In addition, this method requires the quadruple integration of the received signals in Eq. (4), which requires around 40 minutes for the calculation using an Intel Pentium D 2.8 GHz processor. This computation amount is almost the same as in the conventional model. Thus, an acceleration in the imaging speed is also required to use the extended method for 3-dimensional problems.

6. Conclusion

This study proposed an extended imaging algorithm based on aperture synthesis of double scattered waves using the multi-static model. The previous work on the double scattered SAR has been extended to the multi-static configuration. Although this extension is simple and not audacious in itself, the imagery range is substantially improved with the larger real aperture size, especially when using the multiple scattered SAR method. The results of the numerical simulation successfully proves that the proposed model makes the shadow region visible for one of the most difficult target cases, despite the fact that the baseline length is the same for both the conventional and proposed models.

Acknowledgment

This work is supported in part by the Grant-in-Aid for Scientific Research (B) (Grant No. 22360161), and the Grant-in-Aid for Young Scientists (Start-up) (Grant No. 21860036), promoted by Japan Society for the Promotion of Science (JSPS).

References

[1] W.M. Brown, "Synthetic aperture radar," IEEE Trans. Aerosp. Electron. Syst., vol.AES-3, pp.217–229, March 1967.
[2] D. Liu, J. Krolik, and L. Carin, "Electromagnetic target detection in uncertain media: Time-reversal and minimum-variance algorithms," IEEE Trans. Geosci. Remote Sens., vol.45, no.4, pp.934–944, April 2007.
[3] T. Sakamoto and T. Sato, "A target shape estimation algorithm for pulse radar systems based on boundary scattering transform," IEICE Trans. Commun., vol.E87-B, no.5, pp.1357–1365, May 2004.
[4] S. Kidera, T. Sakamoto, and T. Sato, "Accurate UWB radar 3-D Imaging algorithm for complex boundary without range points connections," IEEE Trans. Geosci. Remote Sens., vol.48, no.4, pp.1993–2004, April 2010.
[5] S. Kidera, T. Sakamoto, and T. Sato, "Experimental study of shadow region imaging algorithm with multiple scattered waves for UWB radars," Proc. PIERS 2009, vol.5, no.4, pp.393–396, Aug. 2009.
[6] J.M.F. Moura and Y. Jin, "Detection by time reversal: Single antenna," IEEE Trans. Signal Process., vol.55, no.1, pp.187–201, Jan. 2007.
[7] E.A. Marengo, F.K. Gruber, and A.J. Devaney, "Generalized time-reversal imaging considering multiple scattering effects," IEEE Proc. International Symposium of Antenna & Propagation, vol.2, pp.2087–2090, Aug. 2004.